# Vibrational contribution to static and dynamic (Hyper)polarizabilities of zigzag BN nanotubes calculated by the finite field nuclear relaxation method

**ARTICLE** *in* INTERNATIONAL JOURNAL OF QUANTUM CHEMISTRY · MAY 2012

Impact Factor: 1.43 · DOI: 10.1002/qua.23160



**6 AUTHORS**, INCLUDING:

Matteo Ferrabone
Università degli Studi di Torino
**22** PUBLICATIONS **316** CITATIONS
SEE PROFILE

Valentina Lacivita
Università degli Studi di Torino
**11** PUBLICATIONS **122** CITATIONS
SEE PROFILE

Michel Rérat
Université de Pau et des Pays de l'Adour
**135** PUBLICATIONS **1,925** CITATIONS
SEE PROFILE

Roberto Dovesi
Università degli Studi di Torino
**336** PUBLICATIONS **11,074** CITATIONS
SEE PROFILE

# Vibrational Contribution to Static and Dynamic (Hyper)Polarizabilities of Zigzag BN Nanotubes Calculated by the Finite Field Nuclear Relaxation Method

**MATTEO FERRABONE,[1] BERNARD KIRTMAN,[2] VALENTINA LACIVITA,[1] MICHEL RÉRAT,[3] ROBERTO ORLANDO,[4] ROBERTO DOVESI[1]**

[1]*Dipartimento di Chimica IFM, Università di Torino and NIS-Nanostructured Interfaces and Surfaces - Centre of Excellence, Via P. Giuria 7, 10125 Torino, Italy*
[2]*Department of Chemistry and Biochemistry, University of California, Santa Barbara, California 93106*
[3]*Equipe de Chimie Physique, IPREM UMR5254, Université de Pau et des Pays de l'Adour, 64000 Pau, France*
[4]*Dipartimento di Scienze e Tecnologie Avanzate, Università del Piemonte Orientale, Viale T. Michel 11, 15121 Alessandria, Italy*

*Received 18 April 2011; accepted 25 April 2011*
*Published online in Wiley Online Library (wileyonlinelibrary.com).*
*DOI 10.1002/qua.23160*

**ABSTRACT:** The vibrational contribution to static and dynamic (hyper)polarizabilities for the zigzag $(n,0)$ family of BN nanotubes, with $n$ ranging from (6,0) to (36,0), has been obtained. Calculations were done by the finite field nuclear relaxation (FF-NR) method for periodic systems, newly implemented in the CRYSTAL code, using the Coupled Perturbed Kohn-Sham (CPKS) scheme at the B3LYP/6-31G* level for the required electronic properties. Both transverse and transverse-longitudinal tensor components are determined by applying finite, i.e. static, fields in the transverse direction. The magnitude of the vibrational term increases with the radius of the nanotube as determined by the increase in the field-induced geometric deformation. The resulting vibrational (hyper)polarizability varies from being dominant to negligible, when compared with the corresponding static electronic contribution. This depends upon the radius, as well as the property and the component, in a systematic manner. The extension to longitudinal components, not yet available, will be implemented next.  Int J Quantum Chem 00: 000–000, 2011

**Key words:** BN nanotubes; polarizability and hyperpolarizability; electronic and ionic contributions; Coupled Perturbed Kohn Sham (CPKS); periodic calculations; density functional; B3LYP; gaussian basis sets; CRYSTAL code

*Correspondence to:* M. Rérat; e-mail: michel.rerat@univ-pau.fr

## 1. Introduction

Even before the advent of quantum mechanics, there has been much interest in the various properties exhibited by molecules and materials in response to external electric fields. For spatially uniform perturbing fields, this response is governed by the electric dipole moment or polarization. The dipole moment, in turn, contains permanent and induced components arising from the linear polarizability and the nonlinear hyperpolarizabilities. Each of these properties includes contributions from both the electronic and nuclear motions.

In this article, we will focus on the role of nuclear motions, particularly as they affect both the static and dynamic (hyper)polarizabilities. A major advance in this field occurred about 20 years ago with publication of Bishop and Kirtman's general perturbation treatment (BKPT) [1] based on a double (mechanical and electrical) harmonic initial approximation. They developed closed form expressions for $\omega$-dependent ($\omega$ is the frequency of the electric field) vibrational (hyper)polarizabilities, which are due to vibrational transitions on the Born-Oppenheimer ground electronic state potential energy surface. Although there continue to be many applications of BKPT, the computations can be extensive as they require determination of harmonic and anharmonic vibrational force constants as well as first and higher-order electrical property derivatives. Even in the double harmonic approximation, the calculation of quadratic vibrational force constants can be computationally demanding in many cases.

To streamline the computational effort, an alternative nonperturbative finite field nuclear relaxation (FF-NR) method was proposed about 5 years later by Bishop et al. [2]. The key step in the FF-NR method is a geometry optimization carried out in the presence of a finite, i.e. static, field. This optimization implicitly contains the information about harmonic and anharmonic vibrational parameters needed to obtain vibrational (hyper)polarizabilities. Thus, no force constants or electric property derivatives need to be explicitly calculated. The vibrational properties determined take into account all double harmonic contributions plus all first-order anharmonic terms and, in one case, a second-order anharmonic contribution. A simple extension of the original procedure leads to a treatment that, in principle, can account for all contributions not evaluated in the original FF-NR method [3].

Both static and dynamic vibrational (hyper)polarizabilities are included in the FF-NR method. The latter are obtained within the so-called infinite optical frequency approximation (IOFA), which corresponds to ignoring terms involving $(\omega_v/\omega)^2$ compared with unity. Here, $\omega_v$ is a vibrational frequency and, at typical laser-optical frequencies, the IOFA is found to be well satisfied. Of all the linear and nonlinear optical processes for which the infinite frequency limit is meaningful, the only one not contained in the original formulation is the intensity-dependent refractive index, also known as degenerate four-wave mixing. Recently, a modification has been presented that fills in this lacuna [4]. Finally, it should be noted that the FF-NR method, as well as BKPT, applies specifically to the nonresonant regime. That is to say, it is assumed that the laser-optical frequency may be neglected in comparison with electronic transition frequencies. A response formalism that can be used to calculate the terms that are thereby omitted has recently been presented [5]. However, in the IOFA and in the static limit (the cases studied here), these additional contributions have been shown to vanish [6].

The FF-NR method has been widely applied to molecules. Only very recently, however, it has been utilized for a nanomaterial, namely an infinite periodic $(n,0)$ zigzag BN nanotube [7]. Preliminary coupled perturbed Kohn-Sham (CPKS) calculations were performed for transverse (hyper)polarizabilities of small tubes at the B3LYP level using the CRYSTAL code [8, 9]. In this article, we extend these results to larger nanotubes (up to (36,0)) and to the nondiagonal or mixed tensor components with some exceptions (see next section) due to the fact that the formalism for a finite field in the periodic direction is not yet implemented in the CRYSTAL code. The trends in behavior with increasing radius are explored. As the form of the perturbing operator, as well as its action, is quite different for periodic and non-periodic directions, the convergence of the $(n,0)$ tensor values in the direction orthogonal to the tube axis (nonperiodic direction) toward the h-BN values in a periodic direction represents a strong test of the numerical accuracy and formal consistency of the computational scheme. The effect of the applied field on the band-gap and geometry is also analyzed as a function of the tube radius.

In the next section, we review the FF-NR methodology and provide computational details for treatment of BN nanotubes by means of the CRYSTAL program. Our results are presented and analyzed in

Section 3. Finally, the concluding section contains a summary of key aspects and a discussion of possible further applications/development of the FF-NR method for nanomaterials.

## 2. Method

### 2.1. COMPUTATIONAL DETAILS

The present CPKS calculations of the electronic and vibrational (hyper)polarizabilities were performed with a development version [10] of the periodic ab initio CRYSTAL09 code [9] using the hybrid B3LYP functional, which has proven to be fairly accurate in the determination of band structure and other properties of crystalline systems. DFT exchange-correlation contributions were evaluated by numerical integration over the unit cell volume. In CRYSTAL, radial and angular points of the integration grid are generated through Gauss-Legendre radial quadrature and Lebedev two-dimensional angular point distributions. In our calculations, a (75,974) pruned grid (XLGRID keyword in the CRYSTAL09 manual), corresponding to 75 radial and 974 angular points, was employed. The integration accuracy can be estimated by the error in the electronic charge of the unit cell ($\Delta_e = 2.8 \times 10^{-3}|e|$ out a total of 288 electrons for the (12,0) BNNT). Other details on the grid generation and its influence on the accuracy and cost can be found in Refs. [11–13]. Evaluation of the Coulomb and exact exchange infinite series is controlled by five parameters [9] $(T_1, T_2, T_3, T_4, T_5)$, whose values are set to $T_1 = T_2 = T_3 = T_4 = \frac{1}{2}T_5 = 8$.

Convergence of the self-consistent field (SCF) zeroth-order energy, and first(second) order CPSCF iterations is controlled by the $T_E$ and $T_{CP1(2)}$ parameters, respectively. The SCF cycles are terminated when the difference $\Delta$ between the values of the total energy ($E$, in Hartree) or (hyper)polarizability (in a.u.) per unit, for two successive cycles, is less than $10^{-T_E}$ or $10^{-T_{CP1(2)}}$, respectively. In this study, $T_E = 10$ and $T_{CP1(2)} = 4$. Sometimes the iterations produce large oscillations of the Fock/KS matrices that need to be damped by mixing the matrices of the $n$ and $n-1$ cycles (an FMIXING parameter [9] of 30% and 50% was employed for the SCF and CPSCF cycles, respectively).

A 6-31G* type basis set was used in this study with the exponent of the most diffuse sp shell for each atom energy optimized on the BN monolayer. The effect of the basis set quality, functional and computational parameters on the total energy per BN unit, band gap (BG) and polarizability per BN unit has been documented in Ref. [7]. For the conditions used in this work, there is a difference of less than 2% from the polarizability value obtained with more stringent parameters and a much larger basis set. The choice of basis set is certainly more critical for hyperpolarizabilities. Although no further testing was performed, this basis should be sufficient for our purposes, namely to determine the relative importance of nuclear relaxation vs. electronic contributions for the various hyperpolarizability components as a function of nanotube size.

The CPKS scheme for calculating (hyper)polarizabilities in periodic systems has recently been formulated by generalizing the analogous coupled perturbed Hartree-Fock method. A partial presentation of this generalized procedure has been included in a recent paper [14].

### 2.2. THE FF-NR SCHEME

The electronic (hyper)polarizabilities (with zero-point averaging included) do not take into account so-called "pure" vibrational effects, which can be quite important. The static polarizability, for example, may be approximated as the sum of two terms:

$$\alpha^0 = \alpha^e + \sum_j \frac{\overline{Z}_j^2}{\nu_j^2} \tag{1}$$

where $\alpha^e$ is the electronic contribution, frequently indicated by $\alpha^\infty$; and the (pure) vibrational (sometimes known as ionic) contribution is given, in the double harmonic approximation, by the second term on the right-hand side. In that term, $\overline{Z}_j^2$ is a mass-weighted effective mode Born charge (also known as the dipole derivative in molecular theory) and $\nu_j$ is a harmonic vibrational frequency. The vibrational contribution may alternatively be computed by the FF-NR method without explicitly evaluating either $\overline{Z}_j^2$ or $\nu_j$. As previously shown, [2] the FF-NR result is identical (within numerical accuracy) to that obtained from Eq. (1). In this article, we evaluate not only the static vibrational linear polarizability, $\alpha^0$, but also static and dynamic vibrational hyperpolarizabilities by means of the FF-NR method [2, 3]. This method includes all nonvanishing first-order corrections due to anharmonicity (the first-order correction to $\alpha^0$ vanishes) as well as the double harmonic contribution.

If we denote the equilibrium geometry in a static electric field ($F$) by $R_F$, and $R_0$ without the field, then a Taylor series expansion for the field-dependent dipole moment at the two geometries yields:

$$\mu_t(R_0) = \mu_t(0,R_0) + \sum_u \alpha^e_{tu}F_u + \frac{1}{2}\sum_{u,v}\beta^e_{tuv}F_uF_v + \frac{1}{6}\sum_{u,v,w}\gamma^e_{tuvw}F_uF_vF_w + \cdots \quad (2)$$

and:

$$\mu_t(R_F) = \mu_t(0,R_0) + \sum_u a^\mu_{tu}F_u + \frac{1}{2}\sum_{u,v} b^\mu_{tuv}F_uF_v + \frac{1}{6}\sum_{u,v,w} g^\mu_{tuvw}F_uF_vF_w + \cdots \quad (3)$$

In Eq. (2), the superscript "$e$" refers to the nonresonant value obtained at a sufficiently high frequency that the vibrational contributions to the (hyper)polarizability are negligible. To compare the calculated static value in Eq. (2) with an experimental (hyper)polarizability measured at an optical frequency, the latter must be extrapolated to the zero frequency limit. On the other hand, static field measurements directly yield the coefficients on the right hand side of Eq. (3), assuming that zero-point vibrational averaging effects may be neglected. These coefficients—$a^\mu$, $b^\mu$, and $g^\mu$—contain additional vibrational contributions that are determined by the geometry relaxation induced by the applied static field $F$ (see again Ref. [2]):

$$a^\mu_{tu} = \alpha^e_{tu} + \alpha^{nr}_{tu}(0;0) \quad (4)$$

$$b^\mu_{tuv} = \beta^e_{tuv} + \beta^{nr}_{tuv}(0;0,0) \quad (5)$$

$$g^\mu_{tuvw} = \gamma^e_{tuvw} + \gamma^{nr}_{tuvw}(0;0,0,0) \quad (6)$$

Note that the right-hand side of Eq. (4) is, in principle, identical to the total static polarizability given by Eq. (1) because in either case only harmonic terms are included in the vibrational contribution. However, the static hyperpolarizabilities also contain contributions due to anharmonic force constants and anharmonic electrical property derivatives (see, for example, Ref. [15]). To isolate the nuclear relaxation terms (indicated by the superscript $nr$) one can either subtract the analytically determined electronic term or obtain the difference between Eqs. (2) and (3) numerically. A check of the numerical accuracy of the vibrational contribution to (hyper)polarizabilities will be done on $\alpha^{nr}$ by comparison with the value obtained analytically from Eq. (1).

Similar expansions may be carried out for $\alpha^e$:

$$\alpha^e_{tu}(F,R_0) = \alpha^e_{tu}(0,R_0) + \sum_v \beta^e_{tuv}F_v + \frac{1}{2}\sum_{v,w}\gamma^e_{tuvw}F_vF_w + \cdots \quad (7)$$

$$\alpha^e_{tu}(F,R_F) = \alpha^e_{tu}(0,R_0) + \sum_v b^\alpha_{tuv}F_v + \frac{1}{2}\sum_{v,w} g^\alpha_{tuvw}F_vF_w + \cdots \quad (8)$$

as well as $\beta^e$:

$$\beta^e_{tuv}(F,R_0) = \beta^e_{tuv}(0,R_0) + \sum_w \gamma^e_{tuvw}F_w + \cdots \quad (9)$$

$$\beta^e_{tuv}(F,R_F) = \beta^e_{tuv}(0,R_0) + \sum_w g^\beta_{tuvw}F_w + \cdots \quad (10)$$

where:

$$b^\alpha_{tuv} = \beta^e_{tuv} + \beta^{nr}_{tuv}(-\omega;\omega,0)_{\omega\to\infty} \quad (11)$$

$$g^\alpha_{tuvw} = \gamma^e_{tuvw} + \gamma^{nr}_{tuvw}(-\omega;\omega,0,0)_{\omega\to\infty} \quad (12)$$

$$g^\beta_{tuvw} = \gamma^e_{tuvw} + \gamma^{nr}_{tuvw}(-2\omega;\omega,\omega,0)_{\omega\to\infty} \quad (13)$$

The subscript $\omega \to \infty$ in Eqs. (11)–(13) refers to the IOFA. Strictly speaking, it means that the ratios $(\omega_j/\omega)^2 = (\nu_j/\nu)^2$ are assumed to be negligible compared with unity. In addition to harmonic terms, anharmonic contributions are also included for $\gamma^{nr}_{tuvw}(-\omega;\omega,0,0)_{\omega\to\infty}$ (see Ref. [2]); for the other two nonlinear optical processes the first-order anharmonicity terms vanish. Finally, although not included above (or in this article), the FF-NR method has recently been extended to deal with the intensity dependent refractive index, i.e., $\gamma^{nr}(-\omega;\omega,-\omega,\omega)$, also known as degenerate our wave mixing [4].

The FF-NR method is applied here to obtain the nonzero components of the transverse and mixed longitudinal-transverse vibrational (hyper)polarizabilities. We orient the tube along $x$, the field along $z$, and take into account the fact that all components with an odd number of $z$ (or $y$) indices are null by symmetry. Then, the expansions of $\mu_z$, $\alpha^e_{zz}$, and $\beta^e_{zzz}$ provide the fully diagonal tensor components along $z$ (and $y$, by symmetry). The expansion of $\alpha^e_{xx}$ provides $\gamma^e_{xxzz}$ and $g^\alpha_{xxzz}$; $\alpha^e_{yy}$ provides $\gamma^e_{yyzz}$ and $g^\alpha_{yyzz}$; and $\alpha^e_{xz}$ provides $\beta^e_{xzz}$ and $b^\alpha_{xzz}$. Finally, the expansions of $\beta_{xxz}$ and $\beta_{yyz}$ provide $\gamma^e_{xxzz}$, $g^\beta_{xxzz}$, $\gamma^e_{yyzz}$, and $g^\beta_{yyzz}$. All the non-null tensor components will be reported in the following section.

The FF-NR scheme with field in the periodic $x$ direction is not yet available in the CRYSTAL code, although under implementation. For

**TABLE I**

**Comparison of finite field (FF) with CPKS calculations for transverse component of: (1) $\alpha^e$ and $\gamma^e$ per BN (percentage difference for $\gamma^e$ in parentheses) and (2) static polarizability ($\alpha^0$). Atomic Units.**

| | | *n* | | | | |
|---|---|---|---|---|---|---|
| | | 6 | 12 | 18 | 24 | 36 |
| $\alpha^e_{zz}$ | CPKS | 9.813 | 11.34 | 12.48 | 13.32 | 14.44 |
| | FF$^\mu$ | 9.813 | 11.34 | 12.48 | 13.32 | 14.44 |
| $\alpha^0_{zz}$ | CPKS | 11.56 | 13.66 | 15.49 | 16.93 | 18.99 |
| | FF-NR | 11.56 | 13.66 | 15.49 | 16.94 | 18.96 |
| $\gamma^e_{zzzz}$ | CPKS | 632.3 | 1337 | 2348 | 3391 | 5260 |
| | FF$^\mu$ | 635.5(0.5%) | 1361(1.8%) | 2436(3.7%) | 3490(2.9%) | 5353(1.7%) |
| | FF$^\alpha$ | | 1326(0.8%) | | | |
| | FF$^\beta$ | | 1337(<0.1%) | | | |

The superscripts $\mu$, $\alpha$, and $\beta$ on FF refer to Eqs. (2), (7), and (9), respectively; the CPKS value of $\alpha^0$ was obtained from Eq. (1) and the FF-NR value ($a^\mu$) from Eq. (4).

that reason, tensor components such as $\beta^{nr}_{xxx}(0;0,0)$, $\beta^{nr}_{xxx}(-\omega;\omega,0)_{\omega\to\infty}$, $\beta^{nr}_{xzz}(0;0,0)$, and $\gamma^{nr}_{xxzz}(0;0,0,0)$ cannot be computed at this time.

## 3. Results and discussion

### 3.1. ZERO FIELD CALCULATIONS AND NUMERICAL ACCURACY

The geometries of five $(n,0)$ nanotubes of increasing radius corresponding to $n = 6, 12, 18, 24, 36$ (the number of atoms in the unit cell increases from 24 to 144) were optimized without any field applied. Then, at the field-free equilibrium geometry ($R_0$), the pure electronic quantities $\alpha^e_{zz}$ and $\gamma^e_{zzzz}$ were determined by the analytical CPKS method [10, 14, 16, 17] ($\beta^e$ is null by symmetry). These quantities are indicated as CPKS in Table I. Alternatively, the expansion (at the field-free optimized geometry) of $\mu_z$, $\alpha_{zz}$ and $\beta_{zzz}$ as a function of the field permits us to obtain $\alpha^e_{zz}$ and $\gamma^e_{zzzz}$. The results for the latter derived from the three possible expansions appear as FF$^\mu$ [Eq. (2)], FF$^\alpha$ [Eq. (7)], and FF$^\beta$ [Eq. (9)] in Table I. This shows that the agreement between the two approaches is excellent for $\alpha^e_{zz}$; for $\gamma^e_{zzzz}$ it is very good, in particular when it is derived from the expansion of $\alpha$ (< 1%) or $\beta$ (< 0.1%). The difference is larger when the $\gamma^e_{zzzz}$ value is extracted from the expansion of $\mu_z$, as might be expected for the third-order coefficient, but in the worse case remains smaller than 4%. Overall Table I documents the high accuracy achieved in all cases.

As a final comment, it is worth mentioning that the zero field CPKS calculations of $\alpha$ were performed by fully exploiting the roto-translational symmetry of the tube [18]. The number of symmetry operators varies from 12 to 72 upon going from the (6,0) to the (36,0) nanotube, with a corresponding savings of CPU time. When the field perpendicular to the tube is added, however, the symmetry is lost.

### 3.2. FINITE FIELD NUCLEAR RELAXATION: GEOMETRY OPTIMIZATION

As regards $\alpha^0$, there are two procedures we use to determine this quantity. One way is to compute the full set of harmonic vibrational frequencies by diagonalizing the (zero field) dynamical matrix, which is obtained by numerical differentiation of the analytical energy gradients with respect to atomic cartesian coordinates [19, 20]. These frequencies are, then, combined [see Eq. (1)] with Born charges [21] that are calculated by generating well localized Wannier Functions [22–24]. The other procedure is the FF-NR method [see Eqs. (3) and (4)] which requires field-dependent geometry optimization. For a static field perpendicular to the nanotube, a full geometry optimization was performed starting from the equilibrium geometry at zero field ($R_0 \to R_F$). Then (for all properties including $\alpha^0$), the components of the CPKS dipole moment $\mu$, polarizability $\alpha$, and first hyperpolarizability $\beta$ were calculated at both the field-free geometry $R_0$ and the optimized field-dependent geometry $R_F$. A fit of those quantities gives the vibrational (nuclear relaxation) contributions according to Eqs. (4)–(6) and (11)–(13). Table I shows again that the two approaches for determining the static polarizability $\alpha^0$ [from Eqs. (1) and (3)]

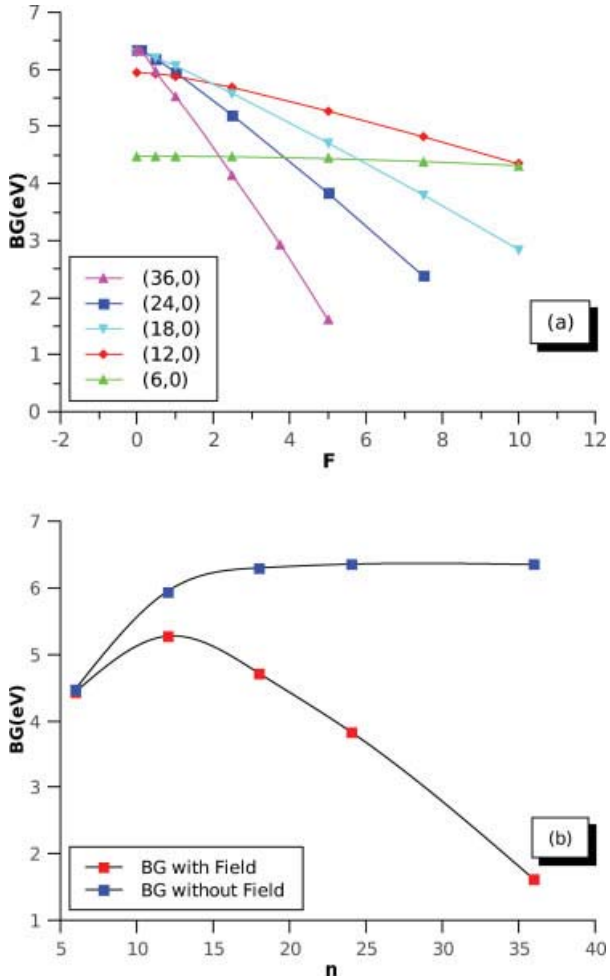


**FIGURE 1.** Band gap (BG, in eV): (a) as a function of field intensity $F$ (in $10^{-3}$ a.u.) and (b) as a function of tube size for field intensity $F = 5 \times 10^{-3}$ a.u. [Color figure can be viewed in the online issue, which is available at wileyonlinelibrary.com.]

are in perfect agreement. Six different field values along the transverse ($z$) direction were considered in the interval 5–100 (in $10^{-4}$ a.u.) for the (6,0), (12,0), and (18,0) tubes, 1–75 for the (24,0) tube and 1–50 for (36,0). The two larger tubes become conducting when fields larger than 100 (for (24,0)) and 60 (for (36,0)) are applied. In Figure 1, the top panel shows that the field reduces the gap (except for $n = 6$) and that the effect sharply increases with the radius of the nanotube. The top panel provides the behavior of the gap as a function of field while the bottom panel compares the zero field value with a given finite field value as a function of $n$.

The geometry deformation of the tube due to the presence of the field is small for the small radius tubes, but becomes important for the more flexible large radius tubes. This is reflected in the relaxation energies per BN unit shown in Figure 2 (see, in particular, the bottom panel). Figure 3 shows how the distance of the B and N atoms lying along the $y$ and $z$ axes ($y$ is perpendicular to both the field direction ($z$) and tube axis) change as a function of the field intensity for the (12,0) and (36,0) tubes. At zero field, B atoms are closer to the tube axis than N atoms by about 0.05 Å in the smaller tube, whereas this difference disappears for the larger tube. As the B and N atoms have opposite charge, they tend to displace in opposite direction when the field is applied. This produces an elongation of the lateral B-N distances parallel to the field, resulting in a large elliptical deformation which increases the radial distance of

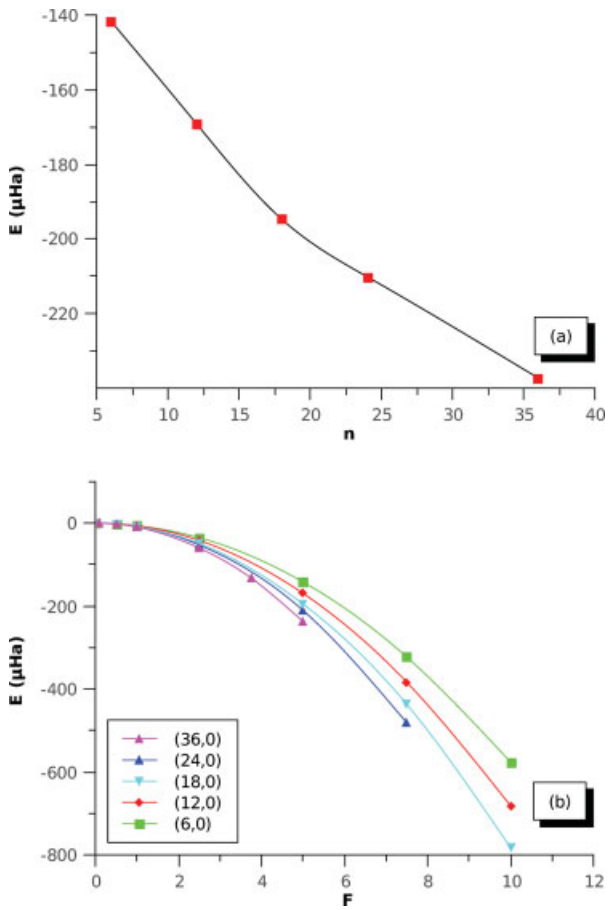


**FIGURE 2.** Energy difference per BN unit (in $\mu$Ha) with respect to unperturbed tubes: (a) as a function of tube size for field intensity $F = 5 \times 10^{-3}$ a.u., and (b) as a function of field intensity $F$ (in $10^{-3}$ a.u.). [Color figure can be viewed in the online issue, which is available at wileyonlinelibrary.com.]

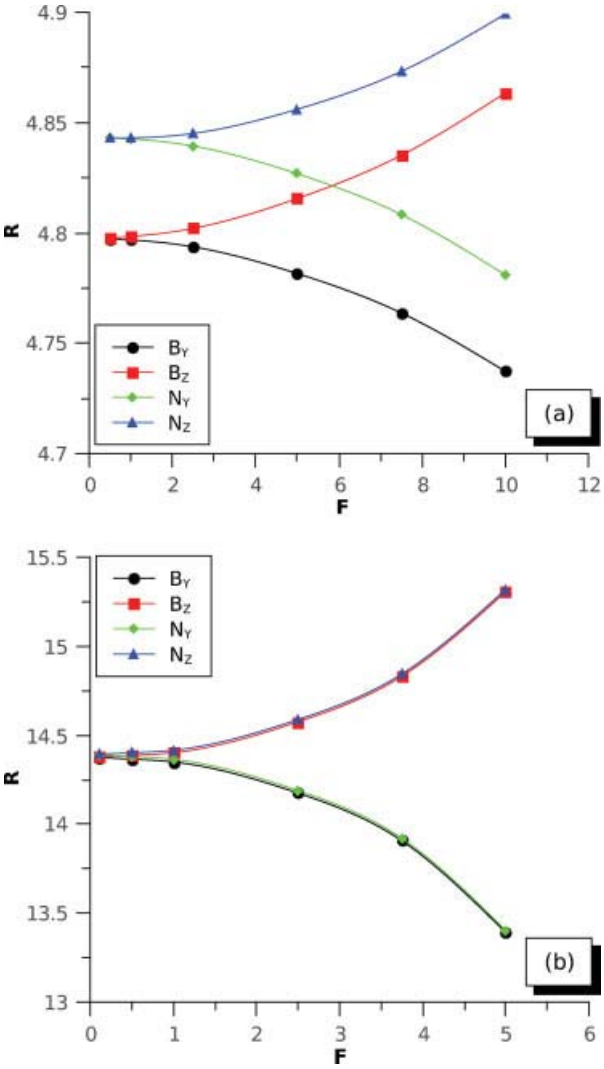


**FIGURE 3.** Geometry relaxation of the (a) (12,0) and (b) (36,0) nanotubes as a function of the field $F$ (in $10^{-3}$ a.u.), which is oriented along the $z$ axis. R (in Å) is the distance from the tube axis of the atoms lying along the field direction ($B_z$ and $N_z$) and in the direction orthogonal to it ($B_y$ and $N_y$). [Color figure can be viewed in the online issue, which is available at wileyonlinelibrary.com.]

both B and N in the field direction ($z$-direction) while decreasing this distance by the same amount in the perpendicular direction ($y$-direction), the cell parameter ($x$-direction) remaining essentially unaltered. The deformation is modest for the (12,0) tube (about 0.05 Å or 1% of the tube radius when the field is $10^{-2}$ a.u.). On the contrary, it is as large as 1 Å or (7% of the tube radius) for the much more flexible (36,0) tube, when a field that is only half as large is applied.

### 3.3. FINITE FIELD NUCLEAR RELAXATION: VIBRATIONAL CONTRIBUTIONS TO TRANSVERSE STATIC AND DYNAMIC SECOND HYPERPOLARIZABILITIES

The procedure to obtain the vibrational nuclear relaxation contributions to the second hyperpolarizabilities is described here in detail using the (6,0) tube as an example. For ease of notation, the nuclear relaxation contributions to $\gamma$ will be labeled $\gamma_n^{nr}$, where $n$ is the number of static fields, so that $\gamma_3^{nr} = \gamma^{nr}(0;0,0,0)$, $\gamma_2^{nr} = \gamma^{nr}(-\omega;\omega,0,0)_{\omega\to\infty}$, and $\gamma_1^{nr} = \gamma^{nr}(-2\omega;\omega,\omega,0)_{\omega\to\infty}$. A plot [see Fig. 4(a)] of $(\mu_z(F,R_F) - \mu_z(0,R_0))/F_z$ versus field along the $z$-direction yields $a_{zz}^{\mu}$ as the intercept and $g_{zzzz}^{\mu}$ as the coefficient of the quadratic term.

As shown previously, the value of $a_{zz}^{\mu}$ obtained from the fit is in perfect agreement with the static polarizability value obtained from Eq. (1) using the Berry phase approach (see Table I). The agreement between the static electronic $\gamma_{zzzz}^{e}$ at $R_0$ obtained separately from the fit to Eqs. (2), (7), and (9) and the analytical CPKS calculation of this same quantity is also very good, allowing us to be confident in our least squares fitting procedure.

From $g_{zzzz}^{\mu} = \gamma_{zzzz}^{e} + \gamma_{3zzzz}^{nr} = 14.6 \times 10^2$ a.u., we obtain a vibrational contribution $\gamma_{3zzzz}^{nr} = (14.6 - 6.32) \times 10^2 = 8.34 \times 10^2$ a.u. where $6.32 \times 10^2$ a.u. is the CPKS value of $\gamma_{zzzz}^{e}$ (see Table I). A plot of $(\alpha_{zz}^{e}(F,R_F) - \alpha_{zz}^{e}(0,R_0))$ versus field is shown in Figure 4(b). In this case, one obtains a pure quadratic function which yields $g_{zzzz}^{\alpha} = \gamma_{zzzz}^{e} + \gamma_{2zzzz}^{nr} = 7.74 \times 10^2$ a.u. Thus, $\gamma_{2zzzz}^{nr} = (7.74 - 6.32) \times 10^2 = 1.42 \times 10^2$ a.u. Finally, Figure 4(c) shows a plot of $(\beta_{zzz}^{e}(F,R_F) - \beta_{zzz}^{e}(0,R_0))$ vs. field. From the slope at zero field, we find $g_{zzzz}^{\beta} = \gamma_{zzzz}^{e} + \gamma_{1zzzz}^{nr} = 4.63 \times 10^2$ a.u. and, hence, $\gamma_{1zzzz}^{nr} = (4.63 - 6.32) \times 10^2 = -1.69 \times 10^2$ a.u. The same scheme has been applied to off-diagonal terms. For example, the development of the CPKS $xx$ polarizability component with respect to the field $F_z$ [Eqs. (7) and (8)] leads to the following expression involving the nondiagonal nuclear relaxation second hyperpolarizability $\gamma_{2xxzz}^{nr}$:

$$\alpha_{xx}^{e}(F,R_F) \simeq \alpha_{xx}^{e}(0,R_0) + \frac{1}{2} g_{xxzz}^{\alpha} F_z^2 \qquad (14)$$

A fit of $\alpha_{xx}^{e}(R_F)$ of the (6,0) nanotube with respect to the field $F_z$ leads to $g_{xxzz}^{\alpha} = -1.63 \times 10^3$ a.u. Then, using Eq. (12) and the CPKS value of $\gamma_{xxzz}^{e}$ ($1.01 \times 10^3$ a.u.), we obtain $\gamma_{2xxzz}^{nr} = -0.62 \times 10^3$ a.u. The value of $\gamma_{1xxzz}^{nr} = -0.54 \times 10^3$ a.u. reported in Table II is obtained from the fit of $\beta_{xxz}^{e}(F,R_F) \simeq g_{xxzz}^{\beta} F_z$ vs. field (alternatively, one could fit $\beta_{xxz}^{e}(F,R_F)/F_z$)

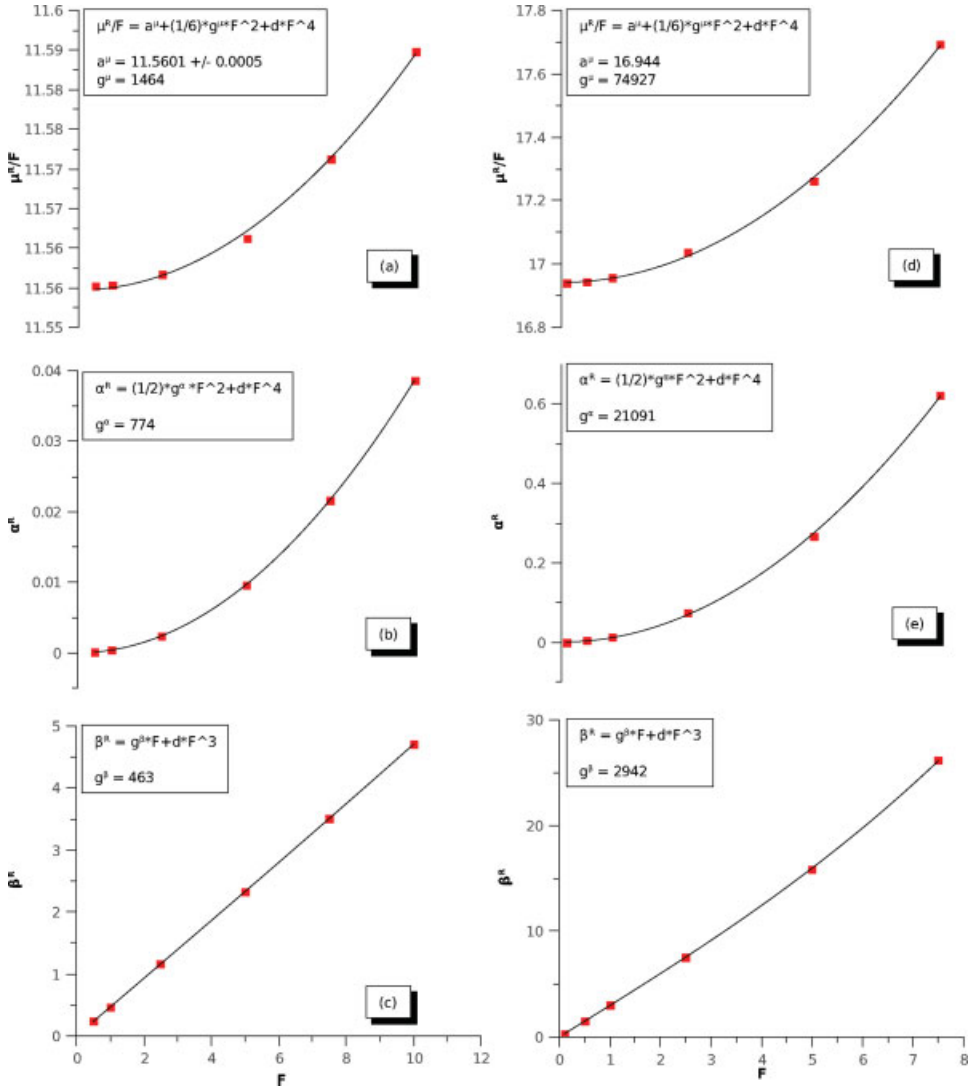


**FIGURE 4.** Dependence of $\mu^R/F = (\mu(F, R_F) - \mu(0, R_0))/F$, $\alpha^R = \alpha^e(F, R_F) - \alpha^e(0, R_0)$ and $\beta^R = \beta^e(F, R_F) - \beta^e(0, R_0)$ with respect to the applied electric field $F$ (in $10^{-3}$ a.u.). The figures to the left [right] refers to the (6,0) [(24,0)] tube. In the inbox of each panel, the fitting function and the values of the fitting parameters are given. [Color figure can be viewed in the online issue, which is available at wileyonlinelibrary.com.]

and Eq. (13) ($\gamma^e_{xxzz}$ from CPKS). Our $\gamma^{nr}_{2yyzz}$ and $\gamma^{nr}_{1yyzz}$ values were obtained in the same way from $\alpha^e_{yy}(F, R_F)$ and $\beta^e_{yyz}(F, R_F)$, respectively. Finally, from the development of the $xz$-component of the polarizability, we obtain the $xzz$-component of the first hyperpolarizability (note that the constant term in the expansion is zero by symmetry):

$$\alpha^e_{xz}(F, R_F) \simeq b^{\alpha}_{xzz} F_z \tag{15}$$

The value reported in Table II for $\beta^{nr}_{1xzz}$, i.e., 0.7 a.u., is obtained by using the CPKS value of $\beta^e_{xzz}$ (21.9 a.u.) and Eq. (11). It is important to bear in mind that the static field(s) in the above always refer to the last 1, 2, or 3 directional indices on the right as indicated by the number 1, 2, or 3 in the label for the given hyperpolarizability.

### 3.4. ELECTRONIC VS. VIBRATIONAL CONTRIBUTION TO THE (HYPER)POLARIZABILITIES AS A FUNCTION OF TUBE SIZE

In this section, we examine how the various vibrational hyperpolarizabilities depend upon the nanotube size and how they compare with the

**TABLE II**

**Electronic and (nuclear relaxation) vibrational contributions to the various (hyper)polarizability components of the $(n, 0)$ BN nanotubes ($n = 6, 12, 18, 24, 36$). Atomic Units.**

| $n$ | 6 | 12 | 18 | 24 | 36 | 44 | 50 |
|---|---|---|---|---|---|---|---|
| $\alpha^e_{xx}$ | 32.1 | 31.3 | 31.1 | 31.0 | 31.0 | 31.0 | 31.0 |
| $\alpha^{nr}_{1xx}$ | 22.3 | 17.9 | 17.6 | 17.5 | 17.4 | 17.3 | 17.3 |
| $\alpha^e_{yy} = \alpha^e_{zz}$ | 9.81 | 11.3 | 12.5 | 13.3 | 14.4 | 14.9 | 15.2 |
| $\alpha^{nr}_{1zz}$ | 1.8 | 2.3 | 3.0 | 3.6 | 4.6 | 5.1 | 5.4 |
| $\beta^e_{xxx}$ | −422 | −359 | −347 | −344 | −343 | −342 | −342 |
| $\beta^e_{xyy} = \beta^e_{xzz}$ | 21.9 | 42.9 | 60.3 | 74.0 | 93.3 | 102 | 108 |
| $\beta^{nr}_{1xzz}$ | 0.7 | 3.9 | 8.2 | 12.3 | 18.5 | | |
| $\gamma^e_{xxxx}$ | 5.36(4) | 4.79(4) | 4.64(4) | 4.56(4) | 4.53(4) | 4.51(4) | 4.50(4) |
| $\gamma^e_{yyyy} = \gamma^e_{zzzz}$ | 6.32(2) | 1.34(3) | 2.35(3) | 3.39(3) | 5.26(3) | 6.30(3) | 6.98(3) |
| $\gamma^{nr}_{1zzzz}$ | −1.69(2) | −0.27(3) | −0.39(3) | −0.45(3) | −0.53(3) | | |
| $\gamma^{nr}_{2zzzz}$ | 1.42(2) | 1.87(3) | 6.82(3) | 17.7(3) | 48.5(3) | | |
| $\gamma^{nr}_{3zzzz}$ | 8.34(2) | 8.24(3) | 34.3(3) | 71.5(3) | 216(3) | | |
| $\gamma^e_{xxyy} = \gamma^e_{xxzz}$ | 1.01(3) | 1.67(3) | 2.34(3) | 2.92(3) | 3.76(3) | 4.18(3) | 4.45(3) |
| $\gamma^{nr}_{1xxzz}$ | −0.54(3) | −0.61(3) | −0.68(3) | −0.71(3) | −0.69(3) | | |
| $\gamma^{nr}_{2xxzz}$ | −0.62(3) | −0.86(3) | −1.47(3) | −1.16(3) | −1.35(3) | | |
| $\gamma^e_{yyzz} = \frac{1}{3}\gamma^e_{zzzz}$ | 2.11(2) | 4.46(2) | 7.83(2) | 1.13(3) | 1.75(3) | 2.10(3) | 2.33(3) |
| $\gamma^{nr}_{1yyzz}$ | −0.46(2) | −0.88(2) | −1.22(2) | −0.14(3) | −0.14(3) | | |
| $\gamma^{nr}_{2yyzz}$ | −3.29(2) | −21.7(2) | −73.7(2) | −17.7(3) | −48.5(3) | | |

All values are per BN unit (power of 10 in parentheses); the static field is along $z$ and $x$ is the longitudinal direction.

corresponding static electronic property. We begin with $\alpha^0_{zz}$ [Eq. (1)] or $a^\mu_{zz}$ [Eq. (4)]. For the (6,0) tube, the electronic $\alpha^e_{zz}$ and total static polarizability $a^\mu_{zz}$ are 9.81 and 11.6 Bohr$^3$, respectively, indicating that the vibrational contribution ($\alpha^{nr}_{zz} = 1.8$ Bohr$^3$) is much smaller than the electronic one. The vibrational contribution increases more rapidly with the size of the nanotube. However, for the (36,0) nanotube (the largest tube for which the FF-NR treatment was applied), the electronic contribution remains substantially larger ($\alpha^e_{zz} = 14.4$ Bohr$^3$ and $a^\mu_{zz} = 19.0$ Bohr$^3$), leading to $\alpha^{nr}_{zz} = 4.6$ Bohr$^3$. In the asymptotic monolayer limit, the ratio increases to roughly 0.50 (see Ref. [7]). At $n = 24$, both the electronic and vibrational contributions are in the saturation regime, i.e. they are increasing sublinearly with $n$ (see Table II).

The case of $\beta_{xzz}$ is qualitatively similar to $\alpha_{zz}$ in the sense that the vibrational $\beta^{nr}_{1xzz}$ is small compared with $\beta^e_{xzz}$ for the (6,0) nanotube but is increasing faster with $n$. For the (36,0) nanotube, the ratio is about 0.20, compared with 0.32 above for $\alpha$, but it is growing somewhat more rapidly. On the other hand, $\beta^e_{xzz}$ is farther than $\alpha^e_{zz}$ from the asymptotic limit. Again, both the electronic and vibrational contributions are in the saturation regime at $n = 24$ (see Table II).

The situation is very different for the static second hyperpolarizability. In that event, the electronic contribution $\gamma^e_{zzzz}$ increases by about a factor 8 (from $6.32 \times 10^2$ to $5.26 \times 10^3$ a.u.), in going from the (6,0) to the (36,0) nanotube, whereas the nuclear relaxation term $\gamma^{nr}_{3zzzz} = g^\mu_{zzzz} - \gamma^e_{zzzz}$ [Eq. (6)] increases by about 260 times ($8.34 \times 10^2$ to $216 \times 10^3$ a.u.). Thus, the ratio between the vibrational and electronic contributions goes from 1.3 to about 40 making the nuclear relaxation contribution dominant for large nanotubes. At $n = 24$, the electronic $\gamma$ is not quite in the saturation regime (it is so at $n = 36$), whereas the static nuclear relaxation $\gamma$ is far from that regime.

We now turn to a comparison of $\gamma^{nr}_{3zzzz}$ with $\gamma^{nr}_{2zzzz}$ and $\gamma^{nr}_{1zzzz}$ (see Table II). As expected, the nuclear relaxation contribution to the dc-Kerr effect (obtained from $g^\alpha_{zzzz}$), although very important, is reduced in comparison with the corresponding contribution to the static vibrational hyperpolarizability (obtained from $g^\mu_{zzzz}$). This is associated with the fact that the number of static fields in the nonlinear process is reduced from 3 to 2 (see Ref. [25]). Thus, $\gamma^{nr}_{2zzzz}$ obtained from Eq. (12) is about $4 - 5$ times smaller than $\gamma^{nr}_{3zzzz}$ (but still as much as an order of magnitude larger than the static electronic term) for all but the (6,0) tube, which is anomalous due to residual strain. $\gamma^{nr}_{1zzzz}$ [obtained from Eq. (13)] is negative and much smaller in absolute value than $\gamma^{nr}_{3zzzz}$ in the (6,0) tube (by about a factor 5). It increases more slowly with $n$ than the other two second hyperpolarizabilities,

so that for the (36,0) nanotube it is about 400 times smaller than $\gamma^{nr}_{3zzzz}$ and 100 times smaller than $\gamma^{nr}_{2zzzz}$. This result is not unexpected as the vibrational contribution to dc second harmonic generation involves just a single static field (note again, the anomalous behavior of the (6,0) tube).

In most instances, the convergence behavior (with increasing $n$) is closely related to the magnitude of the particular (hyper)polarizability term; the larger the magnitude, the slower the convergence to the infinite radius limit. The behavior of the three $\gamma_{zzzz}$ nuclear relaxation contributions as a function of $n$ deserves some additional comment. Figure 5 shows that $\gamma^{nr}_{3zzzz}$ and $\gamma^{nr}_{2zzzz}$ have not reached the saturation regime for the largest (36,0) nanotube studied in this article. These latter components are well represented by a polynomial containing only a cubic power of $n$. On the contrary, $\gamma^{nr}_{1zzzz}$ apparently reaches the saturation tending to $-1.2 \times 10^{-3}$ a.u. at the $n \to \infty$ limit (the numerical noise for $\gamma^{nr}_{1zzzz}$ is larger than for the other two because it is obtained as the difference between large numbers). In this regard, we note that $\gamma^{nr}_{1}$ depends only on the harmonic $[\mu\beta]$ square bracket term (see Ref. [26] for details), whereas $\gamma^{nr}_{2}$ and $\gamma^{nr}_{3}$ depend also on the $[\alpha^2]$ and $[\mu^2\alpha]$ square brackets. The latter square bracket, in particular, is first order in electrical and mechanical anharmonicity while the others are zeroth order (i.e. double harmonic).

The nondiagonal vibrational second hyperpolarizabilities are small in absolute value compared with their static electronic counterparts except for $\gamma^{nr}_{2yyzz}$. In fact, the value of the latter for the (24,0) and (36,0) nanotubes is equal, but opposite in sign, to $\gamma^{nr}_{2zzzz}$. In keeping with our general observation (see above), all of the other nondiagonal vibrational second hyperpolarizabilities lie in the asymptotic regime at $n = 24$. The non-monotonic behavior of $\gamma^{nr}_{2xxzz}$ as a function of $n$ might be due to the fact that for this particular component, the electronic and vibrational contributions are of about the same magnitude, so that the resulting quantity strongly depends on the accuracy of both fits (electronic and vibrational).

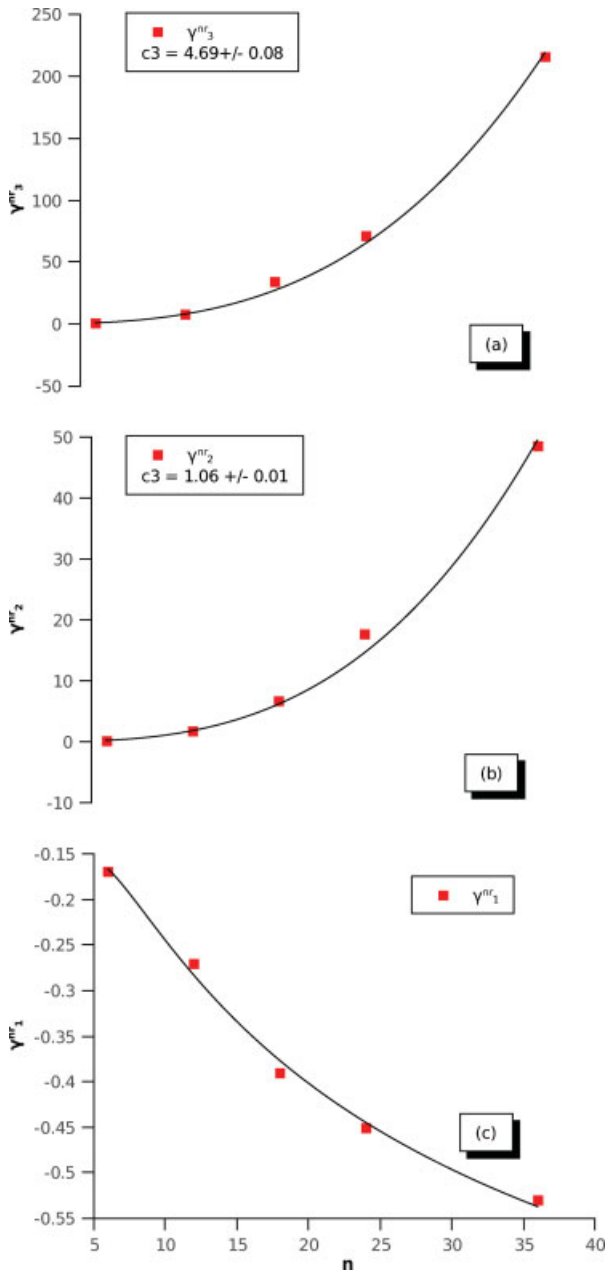


**FIGURE 5.** Dependence of $\gamma^{nr}_{3zzzz}$, $\gamma^{nr}_{2zzzz}$, and $\gamma^{nr}_{1zzzz}$ on the size of the nanotube $n$. The $\gamma^{nr}$ values are all in units of $10^3$ a.u. [Color figure can be viewed in the online issue, which is available at wileyonlinelibrary.com.]

## 4. Conclusions

The vibrational contribution to the static linear polarizability, as well as static and dynamic hyperpolarizabilities, has been evaluated (at the B3LYP/6-31G* level) for zigzag $(n,0)$ BN nanotubes ($n = 6-36$) using the FF-NR scheme. Both transverse and some mixed transverse-longitudinal tensor components are obtained. These calculations were carried out using an extension of the original FF-NR method to periodic systems that has now been implemented for the first time in the CRYSTAL code. The correctness and numerical accuracy of our implementation was checked by comparing: (1) numerical finite field

results with analytical CPKS calculations for the relevant electronic properties, and (2) extrapolated large radius nanotube values with results determined independently for the h-BN infinite layer limit.

The vibrational contribution to each linear/nonlinear property increases with the nanotube radius. This increase is associated with an elliptical field-induced deformation of the cross-sectional geometry, which is enhanced for larger radius tubes due to their greater flexibility, along with a reduced band gap. The rate of increase relative to the corresponding static electronic property is dictated primarily by the number of static fields used to characterize the process. It is also largest for transverse components. Thus, the transverse static vibrational second hyperpolarizability $\gamma^{nr}_{3zzzz} = \gamma^{nr}(0;0,0,0)$ (three static fields) is roughly 1.3 times as large as the corresponding static electronic property for $n = 6, 40$ times as large for $n = 36$, and is still growing supralinearly at that point. The rate of growth in relation to the static electronic property is reduced for two static fields (dc-Kerr effect), and even more so for one field. The ratio is about 0.5, for example, for the transverse linear polarizability in the infinite radius limit.

To obtain the longitudinal components of the vibrational (hyper)polarizability by the FF-NR method, it is necessary to calculate the nuclear relaxation caused by a static longitudinal field. This involves methodology not currently available in the CRYSTAL code, but it is the next step that will be undertaken.

### ACKNOWLEDGMENTS

The authors thank CINECA for granting access to supercomputing resources (ISCRA Award No. HP10AC4ZGA.2010).

## References

1. Kirtman, B.; Bishop, D. Chem Phys Lett 1990, 175, 601.
2. Bishop, D. M.; Hasan, M.; Kirtman, B. J Chem Phys 1995, 103, 4157.
3. Kirtman, B.; Luis, J. M.; Bishop, D. M. J Chem Phys 1998, 108, 10008.
4. Kirtman, B.; Luis, J. M. J Chem Phys 2008, 128, 114101.
5. Hansen, M.; Christiansen, O.; Hattig, C. J Chem Phys 2009, 131, 154101.
6. Kirtman, B.; Luis, J. Int J Quantum Chem 2011, 111, 839.
7. Ferrabone, M.; Kirtman, B.; Orlando, R.; Rérat; Dovesi, R. Accepted on Phys Rev B.
8. Pisani, C.; Dovesi, R.; Roetti, C. Hartree-Fock Ab-initio Treatment of Crystalline Systems; Springer-Verlag: Berlin, 1988.
9. Dovesi, R.; Saunders, V. R.; Roetti, C.; Orlando, R.; Zicovich-Wilson, C. M.; Pascale, F.; Civalleri, B.; Doll, K.; Harrison, N. M.; Bush, I. J.; D'Arco, P.; Llunell, M. CRYSTAL 2009 User's Manual; University of Torino: Torino, 2009.
10. Ferrero, M.; Rérat, M.; Kirtman, B.; Dovesi, R. J Chem Phys 2008, 129, 244110.
11. Pascale, F.; Zicovich-Wilson, C. M.; Orlando, R.; Roetti, C.; Ugliengo, P.; Dovesi, R. J Phys Chem B 2005, 109, 6146.
12. Prencipe, M.; Pascale, F.; Zicovich-Wilson, C.; Saunders, V.; Orlando, R.; Dovesi, R. Phys Chem Min 2004, 31, 559.
13. Tosoni, S.; Pascale, F.; Ugliengo, P.; Orlando, R.; Saunders, V. R.; Dovesi, R. Mol Phys 2005, 103, 2549.
14. Orlando, R.; Lacivita, V.; Bast, R.; Ruud, K. J Chem Phys 2010, 132, 244106.
15. Torrent-Sucarrat, M.; Solá, M.; Duran, M.; Luis, J. M.; Kirtman, B. J Chem Phys 2004, 120, 6346.
16. Ferrero, M.; Rérat, M.; Orlando, R.; Dovesi, R. J Comput Chem 2008, 29, 1450.
17. Ferrero, M.; Rérat, M.; Orlando, R.; Dovesi, R.; Bush, I. J. J Phys Conf Ser 2008, 117, 012016.
18. Noel, Y.; D'Arco, P.; Demichelis, R.; Zicovich-Wilson, C. M.; Dovesi, R. J Comput Chem 2010, 31, 855.
19. Pascale, F.; Zicovich-Wilson, C. M.; Gejo, F. L.; Civalleri, B.; Orlando, R.; Dovesi, R. J Comput Chem 2004, 25, 888.
20. Zicovich-Wilson, C. M.; Pascale, F.; Roetti, C.; Saunders, V. R.; Orlando, R.; Dovesi, R. J Comput Chem 2004, 25, 1873.
21. Ferrabone, M.; Noel, Y.; Wilson, C. Z.; Orlando, R.; Dovesi, R. (in press).
22. Zicovich-Wilson, C. M.; Dovesi, R.; Saunders, V. R. J Chem Phys 2001, 115, 9708.
23. Noel, Y.; Zicovich-Wilson, C. M.; Civalleri, B.; D'arco, P.; Dovesi, R. Phys Rev B 2002, 65, 014111.
24. Zicovich-Wilson, C.; Dovesi, R. In Beyond Standard Quantum Chemistry: Applications from Gas to Condensed Phases, Hernandez-Lamoneda, R., Eds.; Transworld Research Network: Trivandrum, Kerala, India, 2007; vol. 125, p 140.
25. Kirtman, B. Int Conf Comp Meth Sci Eng, AIP Conference Proceedings 2009.
26. Luis, J.; Champagne, B.; Kirtman, B. Int J Quantum Chem 2000, 80, 471.